

Article

Not peer-reviewed version

Parametric Sensitivity of Shear Correction Factors for Multiwall Corrugated Structures

[Julia Graczyk](#), [Jędrzej Tworzydło](#), [Tomasz Garbowski](#)*

Posted Date: 4 February 2026

doi: 10.20944/preprints202602.0323.v1

Keywords: corrugated board; shear correction factor; transverse shear deformation; pixel-based modeling; global sensitivity analysis; latin hypercube sampling



Preprints.org is a free multidisciplinary platform providing preprint service that is dedicated to making early versions of research outputs permanently available and citable. Preprints posted at Preprints.org appear in Web of Science, Crossref, Google Scholar, Scilit, Europe PMC.

Copyright: This open access article is published under a [Creative Commons CC BY 4.0 license](#), which permit the free download, distribution, and reuse, provided that the author and preprint are cited in any reuse.

Disclaimer/Publisher's Note: The statements, opinions, and data contained in all publications are solely those of the individual author(s) and contributor(s) and not of MDPI and/or the editor(s). MDPI and/or the editor(s) disclaim responsibility for any injury to people or property resulting from any ideas, methods, instructions, or products referred to in the content.

Article

Parametric Sensitivity of Shear Correction Factors for Multiwall Corrugated Structures

Julia Graczyk ¹, Jędrzej Tworzydło ² and Tomasz Garbowski ^{3,*}

¹ Institute of Structural Analysis, Poznan University of Technology, Poznan, Poland

² Werner Kenkel Bochnia Spółka z o. o., Bochnia, Poland

³ University Center for Eco-materials, Poznan University of Life Sciences, Poznan, Poland

* Correspondence: tomasz.garbowski@up.poznan.pl

Abstract

Transverse shear deformation plays a non-negligible role in lightweight periodic-core structures and motivates the use of shear-corrected reduced-order plate and beam models. However, the shear correction factor k_s is often treated as a constant despite its strong dependence on cross-sectional heterogeneity and geometry. This work quantifies the global sensitivity of k_s in corrugated paperboard by combining an energy-consistent pixel-based identification of the effective shear stiffness $(GA)_{\text{eff}}$ with a space-filling exploration of the parameter domain. Representative 3-ply (single-wall) and 5-ply (double-wall) configurations are generated directly in the pixel domain using sinusoidal fluting descriptions and non-overlapping liner bands. The effective shear stiffness is obtained from a heterogeneous shear-energy equivalence, where a normalized two-dimensional shear-stress shape function is computed from pixel-based sectional descriptors and integrated with spatially varying shear moduli. Latin Hypercube Sampling is employed to explore wide ranges of flute period, height, and thickness, liner thicknesses, and liner-flute shear-modulus contrasts. Global sensitivity is reported using unit-free normalized indices, including log-elasticities (based on the slope of $\ln k_s$ versus $\ln x$) and partial rank correlation coefficients. The results demonstrate that flute geometry is the primary driver of k_s variability, while material contrast significantly modulates shear-energy localization, particularly in double-wall boards with two distinct flutings. The proposed framework enables high-throughput shear correction assessment and supports robust parameterized reduced-order models for corrugated structures.

Keywords: corrugated board; shear correction factor; transverse shear deformation; pixel-based modeling; global sensitivity analysis; latin hypercube sampling

1. Introduction

Lightweight layered and cellular structures are widely used in engineering whenever high stiffness-to-weight and controllable mechanical response are required. Typical examples include sandwich panels, rib-stiffened shells, corrugated cores, honeycomb configurations, and architected metamaterials. In many applications, the global structural response is governed not only by material properties but also by geometry-driven mechanisms such as local bending of webs, shear deformation within compliant cores, and stress redistribution around voids. As a result, accurate analysis and design require modelling frameworks that can connect microstructural geometry to macroscopic stiffness and strength while remaining computationally efficient for parametric studies and optimization tasks. [1-5]

A common strategy in this context is to replace a detailed heterogeneous configuration with a **homogenized** or **equivalent** continuum model. For layered and periodic structures this often takes the form of an equivalent orthotropic plate or beam, typically derived using energy-based homogenization or computational representative volume elements (RVE). [6-13] While such reduced-

order models offer major computational advantages, their accuracy depends critically on how they represent the internal deformation mechanisms of the original structure. Among these mechanisms, **transverse shear** is particularly challenging: it is negligible for thin homogeneous plates but becomes decisive for thick laminates, soft-core sandwich structures, and periodic cores with voids or inclined webs. [14-20]

In classical plate theory, shear deformation is neglected (Kirchhoff–Love model), leading to good predictions for slender plates dominated by bending. In contrast, in the **Timoshenko–Mindlin** family of models, transverse shear is included and a key parameter appears: the **shear correction factor** k_s . This factor compensates for the fact that the assumed through-thickness shear strain (often constant) does not match the true shear stress distribution, which depends on cross-sectional geometry and material heterogeneity. In homogeneous rectangular beams and plates, reference values of k_s are available (e.g., the well-known factors for rectangular cross-sections). However, for strongly heterogeneous, perforated, or architected cross-sections, k_s cannot be assumed universal and must be identified consistently. [21-26]

The need for reliable shear correction is especially evident in **periodic cores** and multi-layered configurations. For corrugated or honeycomb-like microstructures, shear stresses may localize in thin load paths, bypass void regions, and be redistributed by stiff faces. In such systems, the effective shear response is governed by an interplay of geometry (period, height, thickness, topology) and phase stiffness contrast. Consequently, inaccurate shear correction can lead to systematic errors in predicted deflections, stress resultants, and even in derived design conclusions when simplified plate models are used for parametric design. [27-29]

A second challenge is that shear correction factors are frequently introduced in reduced-order models in a way that is not **energy-consistent**, especially when one attempts to reuse simple textbook factors for cross-sections with complex heterogeneity. Energy-consistent identification is crucial because the effective shear stiffness must reproduce not only the global deflection but also the correct shear energy stored in the structure under transverse loading. For heterogeneous layered systems, energy-based equivalence provides a robust path to define the effective shear stiffness $(GA)_{\text{eff}}$ and to derive k_s relative to an explicit reference model. [10, 26]

A practical difficulty remains: even if an energy-consistent definition is adopted, computing $(GA)_{\text{eff}}$ repeatedly for many design variants can be expensive, particularly if full-scale finite element simulations are required for each geometric configuration. This becomes a bottleneck when the goal is not a single calibration but a systematic assessment of **how sensitive** k_s is to changes in geometry and material properties across a realistic design space. Such sensitivity knowledge is important in at least three contexts: (i) robust design under manufacturing tolerances and paper variability, (ii) development of fast surrogate models for design optimization, and (iii) deciding which parameters must be measured and controlled to ensure predictive reliability of reduced-order models. [30-32]

Corrugated board is a representative and industrially relevant example of such a geometry-dominated, heterogeneous structure. It consists of flat paper liners bonded to one or more sinusoidally shaped fluting layers, forming 3-ply (single-wall) and 5-ply (double-wall) assemblies commonly used in packaging. Corrugated board is simultaneously lightweight, recyclable, and mechanically efficient, yet its response is strongly influenced by flute geometry, paper anisotropy, and moisture-dependent stiffness. Because its internal architecture contains voids and inclined webs, transverse shear deformation may contribute significantly in certain test configurations and structural applications, especially at short spans and under out-of-plane loading. [33-37]

A substantial body of research addresses bending stiffness, edge crush strength, and constitutive modelling of corrugated board under various loading conditions. Reduced-order modelling approaches, including homogenized orthotropic plates, are widely used to predict global stiffness and to support package design. [38, 39] Nevertheless, compared to bending-dominated metrics, the identification and systematic characterization of shear correction remains less developed, particularly for multi-wall boards and for broad variations in geometry and material stiffness that arise across flute families and paper grades.

In addition, sensitivity studies reported in the literature often focus on local effects (small perturbations around a baseline configuration) or on a limited set of parameters. While such analyses

can be informative, they do not necessarily capture the full range of coupled effects present in corrugated structures. When a response is governed by nonlinear geometric interactions, void topology, and stiffness contrast, the ranking of influential parameters may change across the domain. In this case, global sensitivity analysis, based on space-filling sampling strategies such as Latin Hypercube Sampling (LHS), provides a more appropriate framework to evaluate parameter influence, detect interactions, and identify robust trends [31, 40].

Motivated by these gaps, the present work investigates the sensitivity of the shear correction factor k_s for corrugated board across a broad multi-parameter space, focusing on both 3-ply and 5-ply configurations. The study adopts a pixel-based, energy-consistent procedure for computing $(GA)_{\text{eff}}$ directly from the cross-sectional geometry and spatially varying shear modulus fields, avoiding ad-hoc assumptions and enabling high-throughput evaluation [41-47]. The parameter space is explored using LHS, and sensitivity is quantified in a normalized, unit-free manner using measures that directly express percentage-to-percentage influence, enabling an interpretable ranking of drivers across variables with different physical dimensions [10, 35].

The main contributions of this paper are: (a) a global (nonlocal) sensitivity assessment of k_s for corrugated paperboard performed over a wide admissible parameter space, rather than relying on local perturbations around a single reference design. This reveals dominant drivers and interactions relevant for real product families and manufacturing variability; (b) a unified framework for 3-ply and 5-ply boards, explicitly allowing distinct geometries and stiffnesses of two flutings in the double-wall case, which is essential for capturing multi-layer coupling effects that cannot be inferred from single-wall trends; (c) energy-consistent, pixel-based evaluation of $(GA)_{\text{eff}}$ enabling high-throughput computation of k_s across thousands of sampled designs, offering a practical route toward surrogate modelling, robust design, and reliable shear-corrected reduced-order models; (d) Normalized, unit-free sensitivity indices (%/%), based on log-elasticities and complementary global measures, providing directly interpretable statements such as “a 1% change in parameter x produces an average S % change in k_s ” across the explored domain.

These outcomes are important because they help transform k_s from a loosely chosen tuning factor into a geometry- and material-dependent quantity with quantified uncertainty and sensitivity, improving the reliability of reduced-order models used in packaging mechanics and other periodic-core structural applications.

2. Materials and Methods

2.1. Scope of the Study and Investigated Configurations

This study quantifies the sensitivity of the transverse shear correction factor k_s to the key geometric and material parameters of corrugated paperboard. Two structural families are considered: (i) 3-ply (single-wall): top liner + sinusoidal fluting + bottom liner; (ii) 5-ply (double-wall): top liner + fluting 1 + middle liner + fluting 2 + bottom liner.

For the double-wall configuration, the two flutings may exhibit different periods, heights and thicknesses, enabling a systematic evaluation of geometric interactions. The analysis is conducted over a wide admissible parameter space using global sampling (Latin Hypercube), which allows identification of dominant parameters and parameter couplings beyond local perturbations around a single reference design.

2.2. Definition of the Shear Correction Factor

The shear correction factor is defined by comparing the effective transverse shear stiffness of the heterogeneous cross-section with the shear stiffness of a flat reference model:

$$k_s = \frac{(GA)_{\text{eff}}}{G^*A^*}. \quad (1)$$

The reference area is taken as

$$A^* = bH, \quad (2)$$

where b denotes the out-of-plane width (unit width is adopted in computations) and H is the adopted reference height corresponding to the total thickness of the considered corrugated board configuration.

To ensure a stable normalization across broad geometric and material variations, a thickness-weighted reference shear modulus is used:

$$G^* = \sum_{k=1}^{n_\ell} w_k G_k, w_k = \frac{t_k}{\sum_{j=1}^{n_\ell} t_j}, \quad (3)$$

where t_k and G_k are the thickness and shear modulus of the k -th layer (liners and flutings). This definition avoids imposing a priori that only one phase carries shear and ensures consistent comparison between 3-ply and 5-ply configurations.

2.3. Parametric Geometry and Pixel-Based Representation

2.3.1. Sinusoidal Fluting Geometry

The fluting centerline is defined by:

$$z(x) = z_0 + \frac{h}{2} \cos\left(\frac{2\pi}{p}x + \varphi\right), \quad (4)$$

with period p , height h (peak-to-peak), vertical offset z_0 , and phase shift φ . Finite thickness t_f is introduced by constructing a constant-thickness band around the centerline.

For 5-ply boards, two flutings are described independently by (p_1, h_1, t_{f1}) and (p_2, h_2, t_{f2}) and are placed into two non-overlapping core bands between (top, middle) and (middle, bottom) liners, respectively.

2.3.2. Pixel Image Generation and Phase Encoding

The cross-section is represented by a grayscale pixel image generated in MATLAB. The following encoding is used:

- background (void): intensity 1.0,
- liners: intensity 0.5,
- fluting(s): intensity 0.0.

The physical pixel size pix (mm/pixel) controls geometric resolution. To prevent loss of thin layers and boundary artefacts, the admissible domain is constrained such that:

$$t_{\min} \geq 2 \text{ pix}, \quad (5)$$

where t_{\min} is the minimum thickness among all considered liners and flutings. The same generator is employed both for methodological figures and for the numerical evaluation of k_s , ensuring full consistency between geometry visualization and computation.

2.4. Pixel-Based Identification of $(GA)_{\text{eff}}$

2.4.1. Energy-Consistent Formulation

The effective transverse shear stiffness is identified by enforcing equivalence between the shear strain energy of a flat Timoshenko model and the heterogeneous cross-section under the same shear resultant V . For a representative segment of length L , the flat-model energy reads:

$$U_{\text{flat}} = \frac{1}{2} \frac{V^2}{(GA)_{\text{eff}}} L. \quad (6)$$

For a heterogeneous cross-section, the shear energy may be expressed using a normalized 2D shear-stress shape function $\phi(x, z)$ defined such that:

$$\tau_{xz}(x, z) = V \phi(x, z), \int_A \phi(x, z) dA = 1, \quad (7)$$

which guarantees that integration of τ_{xz} over the cross-section yields the shear resultant V . Under linear elasticity, the heterogeneous shear energy becomes:

$$U_{\text{pix}} = \frac{1}{2} \int_A \frac{\tau_{xz}^2(x, z)}{G(x, z)} dA = \frac{1}{2} V^2 \int_A \frac{\phi^2(x, z)}{G(x, z)} dA. \quad (8)$$

By imposing $U_{\text{flat}} = U_{\text{pix}}$, the effective shear stiffness is obtained as:

$$\left(GA \right)_{\text{eff}} = \left(\int_A \frac{\phi^2(x, z)}{G(x, z)} dA \right)^{-1}. \quad (9)$$

Finally, k_s follows from Eq. (1).

2.4.2. Pixel Discretization and Material Mapping

The cross-section is discretized into pixels (or subpixels) of area ΔA . Void pixels are excluded from the mechanical domain. Each material pixel i is assigned a shear modulus G_i based on its phase label (liner vs fluting; in 5-ply cases, fluting 1 and fluting 2 may have different G). This yields a discrete material field $G(x, z) \rightarrow G_i$ and a corresponding set of integration weights ΔA_i .

2.4.3. Construction of the 2D Shear-Stress Shape Function $\phi(x, z)$

To avoid introducing additional modelling assumptions beyond geometry and material phase distribution, the shear-stress shape function $\phi(x, z)$ is constructed directly from the pixelized cross-section using a geometry-consistent 2D formulation. The approach relies on the classical relationship between shear stresses and the first moment of area (static moment) while retaining full 2D resolution required by corrugated geometries.

First, the area and centroid of the material domain are computed from pixel quadrature:

$$A = \int_A 1 dA \approx \sum_{i=1}^{N_p} \Delta A_i, \quad \bar{z} = \frac{1}{A} \int_A z dA \approx \frac{1}{A} \sum_{i=1}^{N_p} z_i \Delta A_i. \quad (10)$$

Next, the second moment of area about the centroidal axis is evaluated:

$$I = \int_A (z - \bar{z})^2 dA \approx \sum_{i=1}^{N_p} (z_i - \bar{z})^2 \Delta A_i. \quad (11)$$

To define the shear-stress distribution across the cross-section, a 2D static-moment field $Q(x, z)$ is introduced. For a point (x, z) in the material domain, $Q(x, z)$ represents the first moment of area of the portion of the cross-section located above that point (with respect to the centroidal axis). In discrete form, for every material pixel i at coordinates (x_i, z_i) , we define:

$$Q_i \equiv Q(x_i, z_i) = \int_{A(z \geq z_i)} (z - \bar{z}) dA \approx \sum_{\substack{j=1 \\ z_j \geq z_i}}^{N_p} (z_j - \bar{z}) \Delta A_j. \quad (12)$$

The local thickness measure entering the shear-stress relation is defined from the pixel domain as an effective local width $b(x, z)$, computed as the material measure in the horizontal direction associated with the given pixel row. In the discretized setting, this can be expressed as:

$$b(z_i) \approx \frac{1}{\Delta z} \sum_{\substack{j=1 \\ z_j \in [z_i - \Delta z/2, z_i + \Delta z/2]}}^{N_p} \Delta A_j, \quad (13)$$

which corresponds to the length of material present at the level $z = z_i$ (for unit out-of-plane width). This definition naturally captures the fact that corrugated sections may be discontinuous along x at a given height due to void regions.

With these ingredients, the unnormalized shear-stress shape field is computed as:

$$\tilde{\phi}_i = \frac{Q_i}{I b(z_i)}. \quad (14)$$

Finally, the field is normalized to satisfy the resultant condition in Eq. (7):

$$\phi_i = \frac{\tilde{\phi}_i}{\sum_{k=1}^{N_p} \tilde{\phi}_k \Delta A_k}. \quad (1)$$

Equations (12)–(15) define a fully 2D, geometry-consistent shape function computed directly from the pixel representation. This construction avoids prescribing shear localization a priori and allows the subsequent energy evaluation to reflect both geometric complexity (corrugation) and spatially varying shear modulus $G(x, z)$.

2.4.4. Discrete Evaluation of $(GA)_{\text{eff}}$ and k_s

With ϕ_i and G_i defined on material pixels, Eq. (9) becomes:

$$(GA)_{\text{eff}} = \left(\sum_{i=1}^{N_p} \frac{\phi_i^2}{G_i} \Delta A_i \right)^{-1}. \quad (16)$$

The shear correction factor is then computed from Eq (1):

All computations are performed for a unit width $b = 1$, and the reported values of k_s are therefore independent of scaling in the out-of-plane direction.

2.5. Global Sensitivity Analysis Using Latin Hypercube Sampling

2.5.1. Parameter Vectors

For the 3-ply configuration, the parameter vector is:

$$\mathbf{x}_3 = [p, h, t_f, t_{L,t}, t_{L,b}, G_f, G_L]. \quad (17)$$

For the 5-ply configuration:

$$\mathbf{x}_5 = [p_1, h_1, t_{f1}, p_2, h_2, t_{f2}, t_{L,t}, t_{L,m}, t_{L,b}, G_{f1}, G_{f2}, G_L]. \quad (18)$$

This parametrization enables separation of geometric and material influences and explicitly allows different flute families in the double-wall board.

2.5.2. Parameter Ranges and Feasibility Constraints

The admissible ranges are selected to cover representative corrugated geometries and material variability while ensuring stable discretization:

3-ply:

- $p \in [4.0, 8.5]\text{mm}$,
- $h \in [1.0, 4.5]\text{mm}$,
- $t_f \in [0.10, 0.35]\text{mm}$,
- $t_{L,t}, t_{L,b} \in [0.10, 0.40]\text{mm}$,
- $G_f \in [0.15, 1.50]\text{GPa}$,
- $G_L \in [0.25, 2.50]\text{GPa}$.

5-ply:

- $p_1, p_2 \in [4.0, 9.5]\text{mm}$,
- $h_1, h_2 \in [1.0, 5.0]\text{mm}$,
- $t_{f1}, t_{f2} \in [0.10, 0.35]\text{mm}$,
- $t_{L,t}, t_{L,m}, t_{L,b} \in [0.10, 0.40]\text{mm}$,
- $G_{f1}, G_{f2} \in [0.15, 1.50]\text{GPa}$,
- $G_L \in [0.25, 2.50]\text{GPa}$.

All samples must satisfy: (i) no overlap of phases (enforced by construction in the image generator), and (ii) the resolution condition in Eq. (5).

2.5.3. LHS Sampling Strategy

A Latin Hypercube Sampling (LHS) design of size N is generated for each configuration family. Geometric variables are sampled from uniform distributions within their bounds. To represent multiplicative uncertainty in stiffness, shear moduli are sampled from a log-uniform distribution:

$$\log G \sim \mathcal{U}(\log G_{\min}, \log G_{\max}). \quad (19)$$

For each sampled vector $\mathbf{x}^{(n)}$, the computational pipeline is:

1. generate pixel geometry,
2. assign shear modulus field G_i ,
3. compute the 2D shape function ϕ_i using Eqs. (12)–(15),
4. evaluate $(GA)_{\text{eff}}$ by Eq. (16),
5. compute k_s by Eq. (1).

This produces the dataset $\{(\mathbf{x}^{(n)}, k_s^{(n)})\}_{n=1}^N$ used in subsequent analysis.

2.5.4. Normalized global sensitivity metrics

To quantify sensitivity in a unit-free and comparable manner across variables, two complementary normalized indices are adopted. First, we use log-elasticities, defined as

$$S_j = \frac{\partial \ln k_s}{\partial \ln x_j}, \quad (20)$$

which directly represent the percentage change of k_s per percentage change of the input variable x_j . In practice, S_j is estimated by fitting a linear model in logarithmic space,

$$\ln k_s = \beta_0 + \sum_{j=1}^d \beta_j \ln x_j + \varepsilon, \quad (21)$$

so that $S_j \approx \beta_j$. Second, we compute partial rank correlation coefficients (PRCC), which quantify the influence of each variable while controlling for the remaining inputs and are robust to monotonic nonlinearities. Both indices are evaluated on the dataset generated by Latin Hypercube Sampling and are reported as normalized, dimensionless sensitivity measures.

2.6. Computational implementation and reproducibility

All calculations are performed in MATLAB. Geometry generation and pixel-based integration are fully automated to enable high-throughput evaluation of k_s across LHS samples. For stochastic designs, a fixed pseudo-random seed is used to ensure reproducibility. A mesh-resolution robustness check is conducted on a representative subset of samples to confirm that the computed k_s values and sensitivity trends are not affected by pixel discretization artefacts.

3. Results

3.1. Dataset overview and numerical stability

Global datasets for 3-ply and 5-ply corrugated boards were generated using Latin Hypercube Sampling (LHS) within the prescribed geometric and material parameter ranges summarized in Table 1. For each LHS realization, the corresponding geometry was constructed directly in the pixel domain, and the shear correction factor k_s was computed using the pixel-based energy-consistent method described in Section 2. After enforcing feasibility and minimum-resolution constraints, the final datasets consisted of N_3 valid samples for the 3-ply configuration and N_5 samples for the 5-ply configuration.

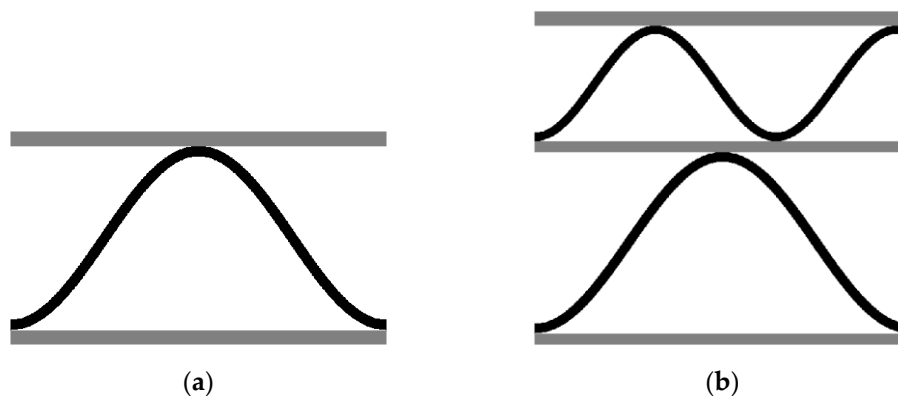


Figure 1. Pixel-based geometry examples generated for the sensitivity study: (a) 3-ply reference geometry and (b) 5-ply example with two distinct flutings. Liners are shown in gray (0.5), fluting(s) in black (0), and background in white (1).

Table 1. Parameter ranges used in the LHS sensitivity study for 3-ply and 5-ply corrugated board. All moduli are sampled log-uniformly; geometric parameters are sampled uniformly. The minimum thickness constraint $t_{\min} \geq 2$ pix is enforced.

Parameter	3-ply		5-ply	
	Min	Max	Min	Max
p [mm]	4.000258	8.499252	4.002924	9.494775
h [mm]	1.001079	4.497692	1.001209	4.998968
t_f [mm]	0.100412	0.349547	0.100012	0.349896
p_2 [mm]	-	-	4.001369	9.498377
h_2 [mm]	-	-	1.000964	4.997345
t_{f2} [mm]	-	-	0.100056	0.349870
$t_{L,t}$ [mm]	0.100053	0.399727	0.100234	0.399820
$t_{L,m}$ [mm]	-	-	0.100245	0.399957
$t_{L,b}$ [mm]	0.100311	0.399791	0.100196	0.399823
G_f [MPa]	0.150515	1.493291	0.150255	1.496948
G_L [MPa]	0.250567	2.498199	0.250230	2.499512

Representative examples of the pixel-based geometries generated within these ranges are shown in Figure 1, illustrating the fundamental structural differences between the single-flute 3-ply board and the double-flute 5-ply configuration.

To verify the numerical robustness of the pixel discretization, a resolution sensitivity study was performed on a representative subset of samples by repeating the computations using a refined pixel size. The relative changes in the shear correction factor, $\Delta k_s/k_s$, are summarized in Table 2.

Table 2. Resolution robustness check: summary statistics of $\Delta k_s/k_s$ (in %) when refining pixel size for a subset of randomly selected samples. Reported are median, 90th percentile, and maximum relative changes.

Dataset	Median [%]	90th percentile [%]	Max [%]
3-ply	0.165672	1.853076	7.497941
5-ply	0.023637	1.082396	7.299894

The limited magnitude of these variations confirms that the global trends discussed in the following sections are not governed by discretization artefacts but reflect genuine geometric and material effects.

3.2. Distribution of the Shear Correction Factor k_s

Across the investigated parameter space, the computed shear correction factors exhibit a pronounced spread, reflecting the strong dependence of transverse shear behavior on both geometry

and material contrast. The empirical distributions obtained from the LHS datasets for the 3-ply and 5-ply configurations are shown in Figure 2.

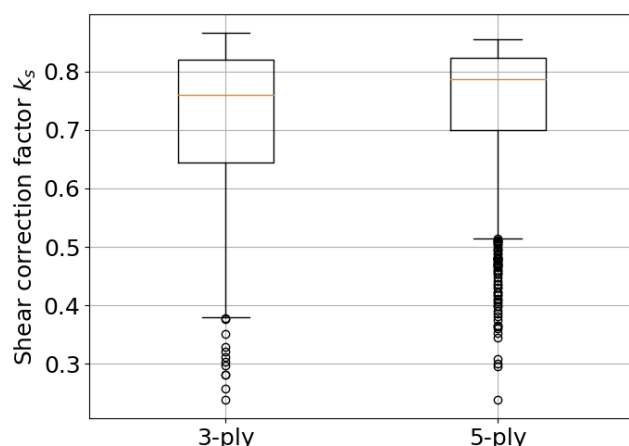


Figure 2. Distribution of k_s obtained from LHS: 3-ply and 5-ply. The histogram/violin representation highlights the spread, skewness, and presence of tails corresponding to extreme geometries or stiffness contrasts.

While the 3-ply boards exhibit a relatively compact distribution, the 5-ply boards display a markedly wider dispersion and heavier tails, as evident in Figure 2(b). A quantitative summary of these distributions is provided in Table 3.

Table 3. Summary statistics of k_s : mean, standard deviation, median, interquartile range (IQR), and selected quantiles (5%, 50%, 95%) for 3-ply and 5-ply datasets.

Dataset	mean	std	median	IQR	q5	q50	q95
3-ply	0.718413	0.128947	0.760203	0.176524	0.466396	0.760203	0.849355
5-ply	0.741803	0.112452	0.787480	0.123227	0.482342	0.787480	0.838569

3.3. Global Sensitivity: Normalized Effects (%/%)

To quantify parameter influence in a unit-free and directly interpretable manner, two complementary global sensitivity measures were employed: (i) log-elasticities (Eq. (20)) and (ii) Partial Rank Correlation Coefficients (PRCC).

The resulting normalized sensitivity indices for the 3-ply and 5-ply configurations are reported in Table 4 and Table 5, respectively.

Table 4. Normalized global sensitivity indices for 3-ply: log-elasticities and PRCC for each input parameter. Positive values indicate an increase of k_s with increasing parameter, negative values indicate a decrease.

Parameter	Log-elasticity	PRCC
p	0.015330	0.074295
h	0.115772	0.530662
t_f	-0.029048	-0.171102
$t_{L,t}$	-0.047826	-0.142491
$t_{L,b}$	-0.064391	-0.195491
G_f	0.023640	0.093608
G_L	-0.010947	-0.056239

Table 5. Normalized global sensitivity indices for 5-ply: log-elasticities and PRCC for each input parameter.

Parameter	Log-elasticity	PRCC
p_1	0.008090	0.019066
h_1	0.049138	0.157244
t_{f1}	-0.005123	0.063589

p_2	0.012620	0.003505
h_2	0.044675	0.144208
t_{f2}	-0.009513	0.061353
$t_{L,t}$	-0.018829	-0.080112
$t_{L,m}$	-0.031460	-0.125244
$t_{L,b}$	-0.021187	-0.091543
G_f	0.019820	0.072902
G_L	-0.006341	-0.031775

For a concise visual ranking of the dominant drivers, the log-elasticities are displayed in the tornado plots shown in Figure 3.

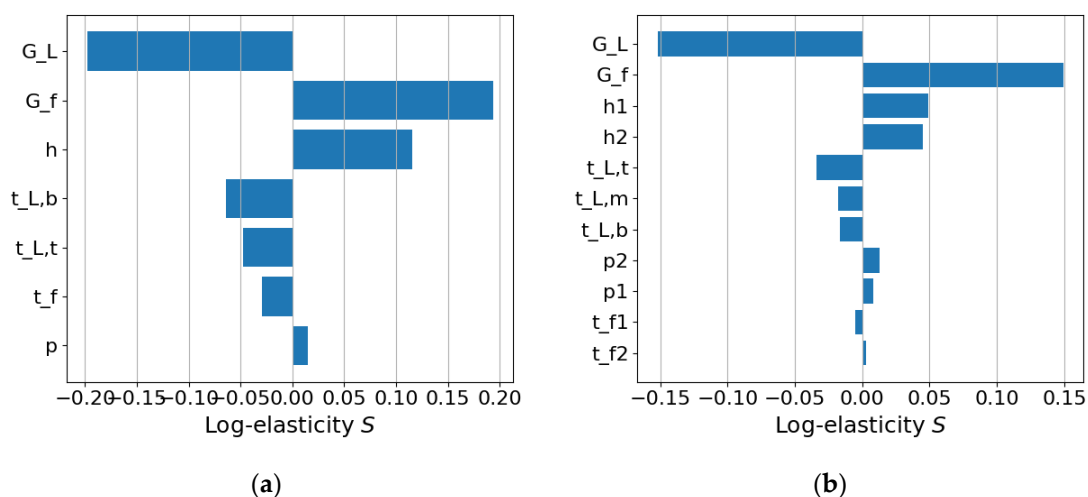


Figure 3. Tornado plots of normalized sensitivities (log-elasticities) ranked by absolute magnitude: (a) 3-ply and (b) 5-ply. This figure provides an immediate ranking of the dominant drivers of k_s across the global parameter space.

3.4. Response surfaces for the dominant geometric drivers

For the 3-ply configuration, the response surface $k_s(p, h)$ evaluated at median values of the remaining parameters is shown in Figure 4.

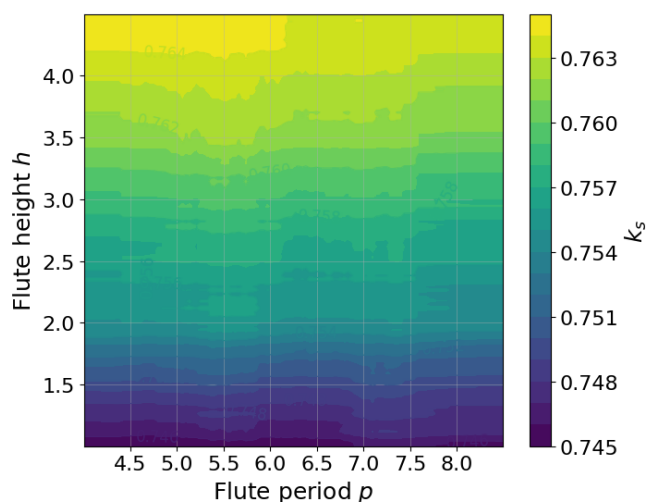


Figure 4. 2D response surface for 3-ply: $k_s(p, h)$ at median values of $(t_f, t_{L,t}, t_{L,b}, G_f, G_L)$. Contours indicate regions of high and low k_s .

Analogous response surfaces for the 5-ply configuration are presented in Figure 5, where each fluting family is examined separately.

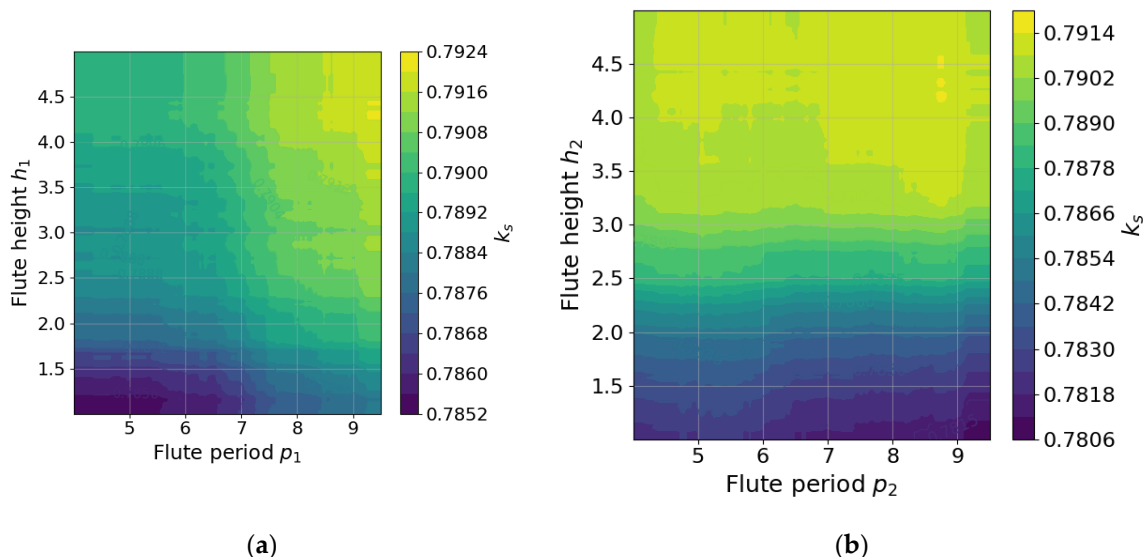


Figure 5. 2D response surfaces for 5-ply: (a) $k_s(p_1, h_1)$ with the second flute fixed at median parameters; (b) $k_s(p_2, h_2)$ with the first flute fixed. These maps highlight how each flute family contributes to the global shear correction behavior.

3.5. Material Contrast Effects and Key Interactions

Material contrast between liners and fluting layers, typically expressed via shear-modulus ratios, significantly affects the shear correction factor. The dependence of k_s on modulus contrast is illustrated in Figure 6.

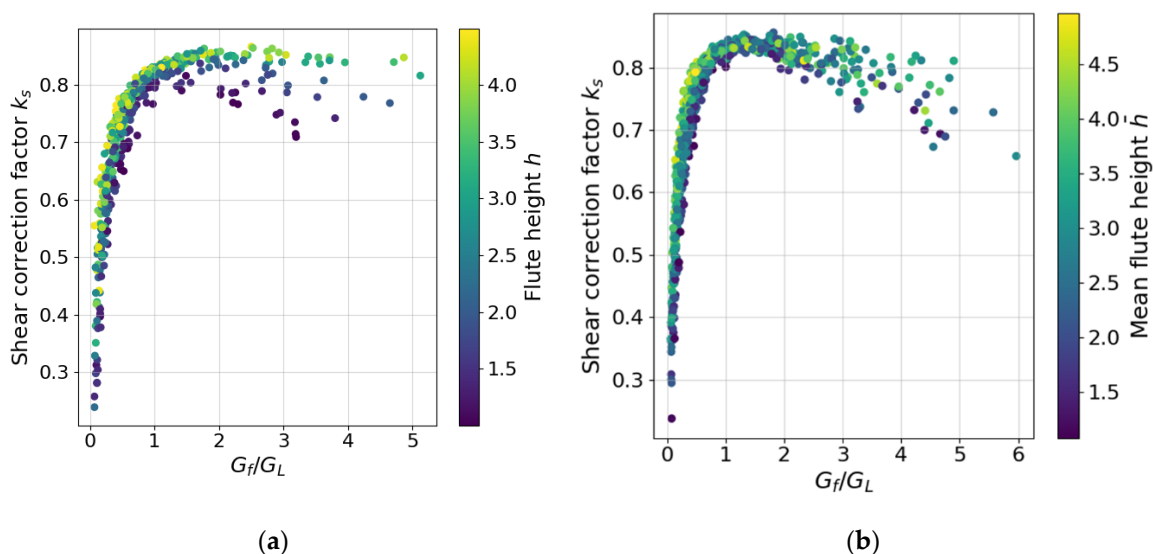


Figure 6. Effect of shear-modulus contrast: scatter of k_s versus G_f/G_L (3-ply) and versus $(G_{f1}/G_L, G_{f2}/G_L)$ (5-ply), with points colored by a dominant geometric variable (e.g., flute height). The plot reveals coupling between stiffness contrast and geometry.

Interaction effects between material contrast and geometry are further examined using binned plots shown in Figure 7.

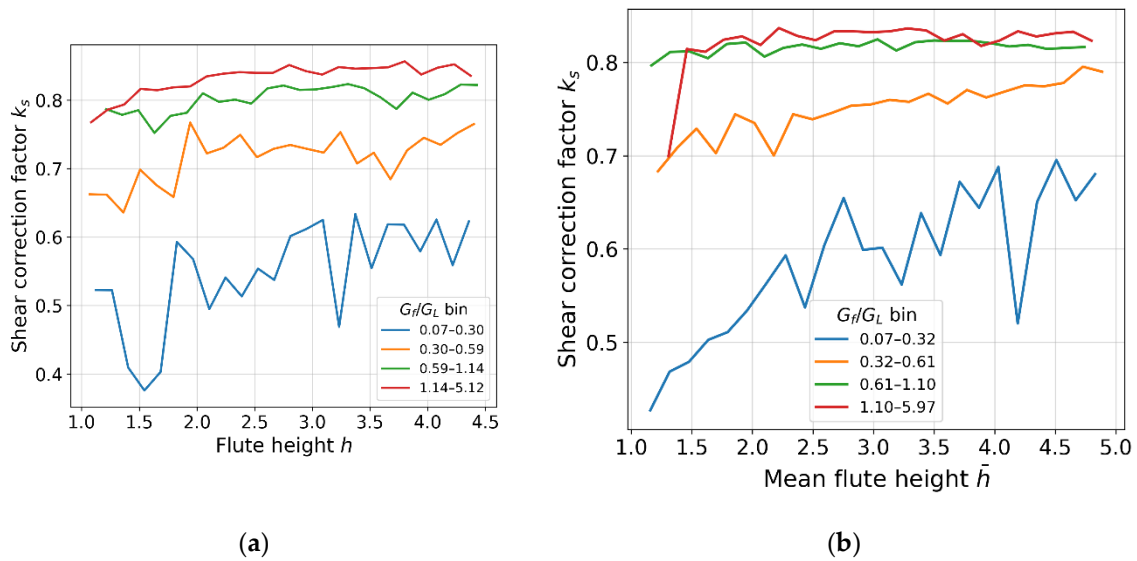


Figure 7. Interaction plot: k_s versus fluted height h for several bins of G_f/G_L for (a) 3-ply and (b) analogous binned plots for 5-ply. The figure illustrates whether stiffness contrast amplifies or suppresses the geometric influence.

3.6. Comparison between 3-ply and 5-ply sensitivity patterns

A direct comparison of normalized sensitivities for the 3-ply and 5-ply configurations is presented in Figure 8, allowing universal and configuration-specific drivers of k_s to be identified.

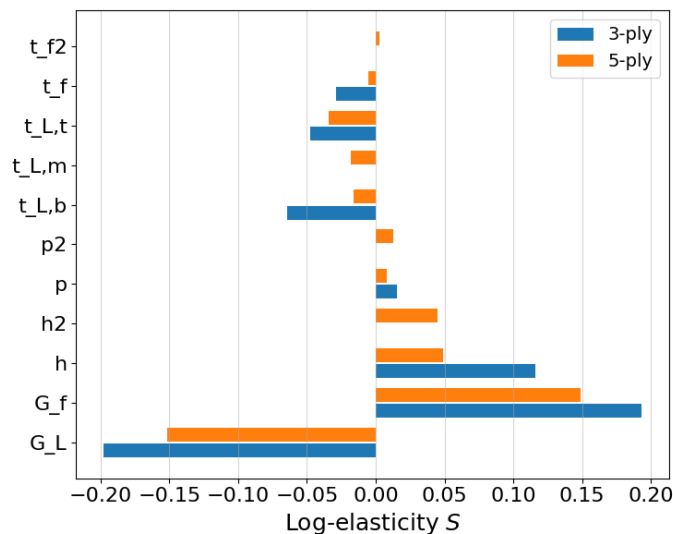


Figure 8. Side-by-side comparison of normalized sensitivities (log-elasticities) for 3-ply and 5-ply. Shared dominant drivers are highlighted, and configuration-specific drivers are identified.

4. Discussion

The present study provides a comprehensive, global assessment of the shear correction factor k_s for multiwall corrugated structures, combining large-scale parametric sampling with an energy-consistent, pixel-based formulation. By systematically analyzing both 3-ply and 5-ply configurations, the results allow clear identification of universal drivers, configuration-specific effects, and key geometric-material interactions governing transverse shear behavior.

4.1. Reliability of the dataset and numerical robustness

A prerequisite for meaningful sensitivity analysis is numerical robustness. The adopted parameter ranges and sampling strategy, summarized in Table 1, ensure broad coverage of realistic

corrugated-board configurations while maintaining physical feasibility. The pixel-based geometries illustrated in Figure 1 confirm that the discretization captures essential geometric features for both single- and double-flute systems.

The resolution sensitivity study reported in Table 2 demonstrates that the computed shear correction factors are only weakly affected by pixel refinement. The small median and upper-percentile deviations indicate that the global trends identified in subsequent analyses are intrinsic to the structural parameters rather than artefacts of discretization. This robustness is particularly important for the 5-ply case, where increased geometric complexity could otherwise amplify numerical sensitivity.

4.2. Global variability of the shear correction factor

The distributions of k_s obtained from Latin Hypercube Sampling, shown in Figure 2, reveal substantial variability across the investigated parameter space. The statistical descriptors provided in Table 3 confirm that this variability is significantly larger for 5-ply boards than for 3-ply boards. This finding reflects the additional deformation mechanisms introduced by the second fluting and the middle liner, which increase both geometric freedom and interaction effects.

The broader dispersion and heavier tails observed in Figure 2(b) indicate that extreme combinations of geometry and material contrast can lead to shear correction factors far from classical reference values. This result directly challenges the common practice of adopting a single, constant shear correction factor for corrugated structures, especially for multiwall configurations.

4.3. Dominant parameters and normalized sensitivity patterns

The normalized sensitivity analysis provides a quantitative ranking of parameter influence in a unit-free form. The results reported in Table 4 (3-ply) and Table 5 (5-ply) show that geometric parameters associated with fluting shape consistently dominate the response. This conclusion is reinforced by the tornado plots in Figure 3, where flute height and period emerge as the primary drivers of k_s across the global parameter space.

While log-elasticities and PRCC largely agree in their ranking, discrepancies for selected parameters suggest the presence of nonlinear or non-monotonic effects. Such behavior is expected in corrugated structures, where local changes in geometry can alter load paths and energy distribution in a non-proportional manner. Importantly, the sensitivity patterns differ between 3-ply and 5-ply boards, indicating that conclusions drawn from single-wall systems cannot be directly transferred to multiwall configurations.

4.4. Physical interpretation via response surfaces

For the 3-ply configuration, the response surface shown in Figure 4 reveals strong nonlinear coupling between flute period and height. Regions of high k_s correspond to geometries that promote more uniform shear strain distribution across the cross-section, whereas low values are associated with slender or widely spaced flutes that concentrate shear deformation.

The 5-ply response surfaces in Figure 5 further demonstrate that each fluting family contributes distinctly to the global shear response. Fixing one flute while varying the other reveals asymmetric influence patterns, highlighting the role of inter-layer interactions. These results confirm that the effective shear correction factor in multiwall boards cannot be interpreted as a simple superposition of individual flute contributions.

4.5. Role of material contrast and interaction effects

Beyond geometry, material contrast between liners and fluting layers plays a critical role in shaping transverse shear behavior. The scatter plots in Figure 6 show that k_s varies systematically with shear-modulus ratios such as G_f/G_L , but the relationship is strongly modulated by geometry. This observation underscores that material contrast alone is insufficient to predict shear correction behavior without considering geometric context.

The interaction plots in Figure 7 provide further insight by demonstrating how stiffness contrast amplifies or suppresses geometric effects. For certain modulus ratios, changes in flute height lead to

pronounced variations in k_s , while for others the response becomes comparatively insensitive. Such interactions explain the partial discrepancies observed between log-elasticities and PRCC in Tables 4 and 5, and they emphasize the need for multidimensional analysis when assessing corrugated-board shear behavior.

4.6. Comparison between 3-ply and 5-ply systems

A direct comparison of normalized sensitivities, presented in Figure 8, highlights both universal and configuration-specific drivers of the shear correction factor. Flute geometry emerges as a universal determinant of k_s across both systems, confirming its fundamental role in transverse shear deformation.

However, the 5-ply configuration exhibits additional influential parameters associated with the middle liner and the second fluting layer. These configuration-specific effects lead to higher variability and more complex interaction patterns, as already suggested by the broader distributions in Figure 2 and the response surfaces in Figure 5. Consequently, design rules or simplified models calibrated for 3-ply boards may be inadequate or even misleading when applied to multiwall corrugated structures.

4.7. Implications for modeling and design

Taken together, the results presented in Figures 1–8 and Tables 1–5 demonstrate that the shear correction factor for corrugated boards is not a fixed material constant but a highly configuration-dependent quantity. The strong sensitivity to geometry, material contrast, and their interactions implies that simplified assumptions, such as adopting a universal shear correction factor, can lead to significant modeling errors, particularly for multiwall systems.

The proposed energy-consistent, pixel-based framework provides a systematic means of quantifying these effects and can serve as a foundation for reduced-order models or design-oriented correlations. Importantly, the distinction between universal and configuration-specific drivers identified in Figure 8 offers guidance for developing simplified yet physically grounded design rules for corrugated structures of varying complexity.

5. Conclusions

This study presented a comprehensive global sensitivity analysis of the shear correction factor k_s for 3-ply and 5-ply corrugated board structures using a pixel-based, energy-consistent numerical framework combined with Latin Hypercube Sampling. Based on the results reported in Tables 1–5 and Figures 1–8, the following conclusions can be drawn:

1. The resolution sensitivity study confirmed that the computed shear correction factors are only weakly affected by pixel refinement. The small relative variations observed for both 3-ply and 5-ply configurations demonstrate that the identified trends are intrinsic to the structural parameters rather than discretization artefacts, supporting the reliability of the proposed methodology.
2. The distributions of k_s reveal substantial variability across the investigated parameter space, with significantly broader ranges for 5-ply boards compared to 3-ply boards. This increased dispersion reflects the additional deformation mechanisms and interaction effects introduced by multiple flutings and intermediate liners, indicating that k_s cannot be treated as a universal constant.
3. Normalized sensitivity indices consistently identify fluting geometry—particularly flute height and period—as the primary drivers of the shear correction factor in both configurations. These parameters exert a stronger influence on k_s than material properties alone, underscoring the central role of geometric design in governing transverse shear behavior.
4. Response surfaces and interaction plots demonstrate pronounced nonlinear coupling between geometric parameters as well as between geometry and material contrast. In multiwall configurations, the contribution of each fluting family is not additive, and interactions between layers play a decisive role in shaping the effective shear response.
5. While shear-modulus ratios between fluting and liners significantly affect k_s , their influence is strongly dependent on the underlying geometry. Material contrast can either amplify or suppress

geometric effects, explaining observed differences between sensitivity measures and reinforcing the need for multidimensional analysis.

6. Although certain drivers of k_s , such as fluting geometry, are universal, multiwall (5-ply) boards exhibit additional configuration-specific sensitivities associated with the middle liner and the second fluting layer. Consequently, conclusions drawn from single-wall systems cannot be directly extrapolated to more complex corrugated structures.
7. The results demonstrate that adopting a single, fixed shear correction factor—commonly used in simplified beam and plate models—may lead to significant inaccuracies, particularly for multiwall corrugated boards. The presented framework provides a physically grounded basis for developing configuration-dependent shear correction factors suitable for advanced numerical modeling and design-oriented reduced-order formulations.

Overall, this work establishes a systematic methodology for quantifying the sensitivity of shear correction factors in corrugated structures and provides new insight into the interplay between geometry and material contrast. The findings offer a foundation for improved mechanical modeling of multiwall corrugated boards and motivate the development of refined design rules that account explicitly for structural configuration.

Author Contributions: Conceptualization, J.G. and T.G.; methodology, J.G. and T.G.; software, T.G.; validation, J.G., J.T. and T.G.; formal analysis, J.G.; investigation, J.G.; resources, J.T.; data curation, J.T.; writing—original draft preparation, J.G. and T.G.; writing—review and editing, J.T.; visualization, J.G. and T.G.; supervision, T.G.; project administration, T.G.; funding acquisition, T.G. All authors have read and agreed to the published version of the manuscript.

Funding: The work uses the results of research carried out as part of the project implemented by the company WERNER KENKEL Bochnia Spółka z o. o. The project was funded within the grant of The National Centre for Research and Development under the number POIR.01.01.01-00-0002/21.

Institutional Review Board Statement: Not applicable.

Informed Consent Statement: Not applicable.

Data Availability Statement: The data supporting the findings of this study are available from the corresponding author upon reasonable request.

Acknowledgments: The authors thank WERNER KENKEL Bochnia Sp. z o.o. for providing technical support and help in data interpretation.

Conflicts of Interest: The authors declare no conflicts of interest.

References

1. Gibson, L.J.; Ashby, M.F. *Cellular Solids: Structure and Properties*, 2nd ed.; Cambridge University Press: Cambridge, UK, 1997.
2. Fleck, N.A.; Deshpande, V.S.; Ashby, M.F. Micro-architected materials: Past, present and future. *Proc. R. Soc. A* **2010**, *466*.
3. Wadley, H.N.G. Multifunctional periodic cellular metals. *Philos. Trans. R. Soc. A* **2006**, *364*.
4. Schaedler, T.A.; Carter, W.B. Architected Cellular Materials. *Annu. Rev. Mater. Res.* **2016**, *46*.
5. Nemat-Nasser, S.; Hori, M. *Micromechanics: Overall Properties of Heterogeneous Materials*; Elsevier: Amsterdam, The Netherlands, **1993**.
6. Biancolini, M.E. Evaluation of equivalent stiffness properties of corrugated board. *Compos. Struct.* **2005**, *69*.
7. Talbi, N.; Batti, A.; Ayad, R.; Guo, Y.Q. An analytical homogenization model for finite element modelling of corrugated cardboard. *Compos. Struct.* **2009**, *88*.
8. Buannic, N.; Cartraud, P.; Quesnel, T. Homogenization of corrugated core sandwich panels. *Compos. Struct.* **2003**, *59*.
9. Suquet, P. Elements of homogenization for inelastic solid mechanics. In *Homogenization Techniques for Composite Media*; Sanchez-Palencia, E., Zaoui, A., Eds.; Springer: Berlin/Heidelberg, Germany, **1987**.

10. Garbowski, T.; Gajewski, T. Determination of transverse shear stiffness of sandwich panels with a corrugated core by numerical homogenization. *Materials* **2021**, *14*.
11. Maouche, M.-F.; Hecini, M. Analytical Homogenization Approach for Double-Wall Corrugated Cardboard Incorporating Constituent Layer Characterization. *Appl. Mech.* **2026**, *7*, 4. <https://doi.org/10.3390/applmech7010004>.
12. Beck, M.; Fischerauer, G. Modeling Warp in Corrugated Cardboard Based on Homogenization Techniques for In-Process Measurement Applications. *Appl. Sci.* **2022**, *12*, 1684. <https://doi.org/10.3390/app12031684>.
13. Aduke, R.N.; Venter, M.P.; Coetzee, C.J. An Analysis of Numerical Homogenisation Methods Applied on Corrugated Paperboard. *Math. Comput. Appl.* **2023**, *28*, 46. <https://doi.org/10.3390/mca28020046>.
14. Reissner, E. The effect of transverse shear deformation on the bending of elastic plates. *J. Appl. Mech.* **1945**, *12*.
15. Mindlin, R.D. Influence of rotatory inertia and shear on flexural motions of isotropic, elastic plates. *J. Appl. Mech.* **1951**, *18*.
16. Reddy, J.N. A simple higher-order theory for laminated composite plates. *J. Appl. Mech.* **1984**, *51*.
17. Touratier, M. An efficient standard plate theory. *Int. J. Eng. Sci.* **1991**, *29*.
18. Shimpi, R.P. Refined plate theory and its variants. *AIAA J.* **2002**, *40*.
19. Thai, H.T.; Choi, D.H. A refined shear deformation theory for free vibration of functionally graded plates. *Compos. Part B Eng.* **2012**, *43*.
20. Sayyad, A.S.; Ghugal, Y.M. On the free vibration of angle-ply laminated composite and soft core sandwich plates. *J. Sandwich Struct. Mater.* **2017**, *19*.
21. Cowper, G.R. The shear coefficient in Timoshenko's beam theory. *J. Appl. Mech.* **1966**, *33*.
22. Gruttmann, F.; Wagner, W. Shear correction factors in Timoshenko's beam theory for arbitrary shaped cross-sections. *Comput. Mech.* **2001**, *27*.
23. Pai, P.F. A new look at shear correction factors and warping functions of anisotropic laminates. *Int. J. Solids Struct.* **1995**, *32*.
24. Nguyen, T.-K.; Vo, T.P.; Thai, H.-T. Vibration and buckling analysis of functionally graded sandwich plates with improved transverse shear stiffness based on the first-order shear deformation theory. *Proc. Inst. Mech. Eng. Part C J. Mech. Eng. Sci.* **2014**, *228*.
25. Vinson, J.R. *The Behavior of Sandwich Structures of Isotropic and Composite Materials*; CRC Press: Boca Raton, FL, USA, 1999.
26. Zenkert, D. *The Handbook of Sandwich Construction*; EMAS: West Midlands, UK, 1997.
27. Nordstrand, T.; Carlsson, L.A. Evaluation of transverse shear stiffness of structural core sandwich plates. *Compos. Struct.* **1997**, *37*.
28. Östlund, S.; Niskanen, K., Eds. *Mechanics of Paper Products*, 2nd ed.; Walter de Gruyter: Berlin, Germany, **2021**.
29. Hägglund, R.; Isaksson, P. A mechanical model for paper and other planar fiber networks. *Mech. Mater.* **2006**, *38*.
30. Saltelli, A.; Ratto, M.; Andres, T.; Campolongo, F.; Cariboni, J.; Gatelli, D.; Saisana, M.; Tarantola, S. *Global Sensitivity Analysis: The Primer*; Wiley: Chichester, UK, **2008**.
31. Helton, J.C.; Davis, F.J. Latin hypercube sampling and the propagation of uncertainty in analyses of complex systems. *Reliab. Eng. Syst. Saf.* **2003**, *81*.
32. Sudret, B. Global sensitivity analysis using polynomial chaos expansions. *Reliab. Eng. Syst. Saf.* **2008**, *93*.
33. Mrówczyński, D.; Gajewski, T.; Garbowski, T. Sensitivity Analysis of Creasing Parameters in Corrugated Board. *Materials* **2023**, *16*.
34. Suarez, B.; Muneta, L.M.; Romero, G.; Sanz-Bobi, J.D. Efficient Design of Thin Wall Seating Made of a Single Piece of Heavy-Duty Corrugated Cardboard. *Materials* **2021**, *14*, 6645. <https://doi.org/10.3390/ma14216645>.
35. Rogalka, M.; Grabski, J.K.; Garbowski, T. Identification of Geometric Features of the Corrugated Board Using Images and Genetic Algorithm. *Sensors* **2023**, *23*.
36. Rogalka, M.; Grabski, J.K.; Garbowski, T. Deciphering Double-Walled Corrugated Board Geometry Using Image Analysis and Genetic Algorithms. *Sensors* **2024**, *24*.

37. Rogalka, M.; Grabski, J.K.; Garbowski, T. In-Situ Classification of Highly Deformed Corrugated Board Using Convolution Neural Networks. *Sensors* **2024**, *24*.
38. Aduke, R.N.; Venter, M.P.; Coetzee, C.J. Numerical Modelling of Corrugated Paperboard Boxes. *Math. Comput. Appl.* **2024**, *29*, 70. <https://doi.org/10.3390/mca29040070>.
39. Staszak, N.; Garbowski, T.; Szymczak-Graczyk, A. Solid Truss to Shell Numerical Homogenization of Prefabricated Composite Slabs. *Materials* **2021**, *14*, 4120. <https://doi.org/10.3390/ma14154120>
40. Vu-Bac, N.; Rafiee, R.; Zhuang, X.; Lahmer, T.; Rabczuk, T. Uncertainty quantification for multiscale modeling of polymer nanocomposites with correlated parameters. *Compos. Part B Eng.* **2015**, *68*.
41. Garbowski, T.; Graczyk, J. Shear correction factor in corrugated board layered plates. *Polish Paper Rev.* **2025**, *81*, 686–690. <https://doi.org/10.15199/54.2025.12.3>
42. Graczyk, J.; Gajewski, T.; Garbowski, T. Shear Correction Factor for Porous Eco-Materials: Mechanical Characterization of a Heterogeneous Medium. *Preprints* **2026**, 2026011251. <https://doi.org/10.20944/preprints202601.1251.v1>
43. Graczyk, J.; Gajewski, T.; Garbowski, T. Numerical Determination of the Shear Correction Factor for Thin-Walled Steel Sections Using Shell-Based Finite Element Modeling. *SSRN* **2026** <https://doi.org/10.2139/ssrn.6144980>
44. Szymczak-Graczyk, A.; Guri, Z.; Canaj, I.; Garbowski, T. Generalized Shear Correction Factor for Non-Homogeneous Beam Cross-Sections with an Embedded Steel Core. *Preprints* **2026**, xxx. <https://doi.org/10.20944/preprints202601.xxxx.v1>
45. Loja, M.A.R.; Barbosa, J.I. Exponentially Graded Auxetic Structures: An Assessment of the Shear Correction Factor and Static Deflection. *Appl. Sci.* **2024**, *14*, 9356. <https://doi.org/10.3390/app14209356>
46. Mota, A.F.; Loja, M.A.R.; Barbosa, J.I.; Rodrigues, J.A. Porous Functionally Graded Plates: An Assessment of the Influence of Shear Correction Factor on Static Behavior. *Math. Comput. Appl.* **2020**, *25*, 25. <https://doi.org/10.3390/mca25020025>
47. Staszak, N.; Szymczak-Graczyk, A.; Garbowski, T. Elastic Analysis of Three-Layer Concrete Slab Based on Numerical Homogenization with an Analytical Shear Correction Factor. *Appl. Sci.* **2022**, *12*, 9918. <https://doi.org/10.3390/app12199918>

Disclaimer/Publisher's Note: The statements, opinions and data contained in all publications are solely those of the individual author(s) and contributor(s) and not of MDPI and/or the editor(s). MDPI and/or the editor(s) disclaim responsibility for any injury to people or property resulting from any ideas, methods, instructions or products referred to in the content.